CrossMark

A Catalog of Known Galactic K-M Stars of Class I Candidate Red Supergiants in *Gaia* DR2

M. Messineo[1] and A. G. A. Brown[2]

[1] Key Laboratory for Researches in Galaxies and Cosmology, University of Science and Technology of China, Chinese Academy of Sciences, Hefei, Anhui, 230026, People's Republic of China; messineo@ustc.edu.cn
[2] Leiden Observatory, Leiden University, Niels Bohrweg 2, 2333 CA Leiden, The Netherlands

Abstract

We investigate individual distances and luminosities of a sample of 889 nearby candidate red supergiants (RSGs) with reliable parallaxes ($\varpi/\sigma_\varpi > 4$ and RUWE < 2.7) from *Gaia* Data Release 2 (DR2). The sample was extracted from the historical compilation of spectroscopically derived spectral types by Skiff, and consists of K-M stars that are listed with class I at least once. The sample includes well-known RSGs from Humphreys, Elias et al., Jura & Kleinmann, and Levesque et al. Infrared and optical measurements from the Two Micron All Sky Survey, Catalog of Infrared Observations (CIO), *Midcourse Space Experiment*, *Wide-field Infrared Survey Explorer*, MIPSGAL, Galactic Legacy Infrared Midplane Extraordinaire (GLIMPSE), and The Naval Observatory Merged Astrometric Dataset catalogs allow us to estimate the stellar bolometric magnitudes. We analyze the stars in the luminosity versus effective temperature plane and confirm that 43 sources are highly probably RSGs with $M_{bol} < -7.1$ mag. Of the stars in the sample, 43% have masses $>7\,M_\odot$. Another $\approx$30% of the sample consists of giant stars.

Key words: infrared: stars – stars: evolution – stars: massive – supergiants

Supporting material: machine-readable tables

1. Introduction

The Milky Way is the closest laboratory for resolved stellar populations and a prototype of spiral galaxies. Nonetheless, our position within the disk and dust obscuration render its study difficult. Red supergiants (RSGs) are the brightest stars seen at infrared wavelengths because they are young and cold objects with typical luminosities above $10^4\,L_\odot$. RSGs are tracers of stellar populations from 4 to 30 Myr, with masses from about 9 to 40 $M_\odot$ (e.g., Ekström et al. 2012; Chieffi & Limongi 2013); from their numbers and luminosities one can evaluate Galactic star formation in this range of time. The distribution of known spectral types of Galactic RSGs peaks at spectral types M0–M2 (Elias et al. 1985; Davies et al. 2007).

Having said that, the current census of RSGs, including M types, is highly incomplete, with little being known about their spatial distribution (see, for example, Davies et al. 2009; Messineo et al. 2016). At optical wavelengths, catalogs of RSGs have been compiled by locating bright late-type stars in the directions of OB associations. Humphreys (1978) listed 92 RSGs, Elias et al. (1985) listed 90 RSGs, Levesque et al. (2005) analyzed the spectra of 62 RSGs, Jura & Kleinmann (1990) listed $\approx$135 RSGs, and Gehrz (1989) predicted at least 5000 RSGs. Overall, less than 1000 Galactic late-type stars of class I are known, with only about 400 RSGs. Their detection is extremely difficult because their colors are similar to those of giant late-type stars and knowledge on their distances is poor, and because their colors and magnitudes overlap with those of the more numerous asymptotic giant branch (AGB) stars (from low masses to super-AGBs of 9–10 $M_\odot$). Furthermore, even though associations and clusters make it easier to detect massive stars, it appears that only $\approx$2% of inner Galaxy supergiants are associated with stellar clusters (Messineo et al. 2017). Pulsation properties and chemical abundances are

required for identifying the stage of evolution and the nuclear burning that has occurred.

Gaia data allow us to classify individual stars by providing their distances. We prepared a catalog of bright late-type stars reported at least once with class I, i.e., as stars of K- or M-type and luminosity class I in the spectroscopic catalog of Skiff (2014), and with data from *Gaia* DR2. Historical spectroscopic records provided spectral types that in combination with *Gaia* parallaxes and photometric data enabled us to measure the stellar luminosities. With that in hand, we were able to extract a catalog of genuine stars of luminosity class I and to derive average magnitudes per spectral type. In Section 2, we describe the sample, their parallaxes, and available infrared measurements. In Section 3, we estimate the stellar luminosities and provide average values per spectral type. In Section 4, we summarize the results of our exercise.

2. Observational Data

2.1. The Sample and Available Spectral Types

We compiled a list of about 1400 K-M stars of class I with latitudes $|b| < 10°$ from the historical records of stellar spectral types by Skiff (2014).[3] All late-type stars with at least one classification as luminosity class I were retained. In addition, we cross-matched Skiff's list with existing Galactic compilations of RSGs, e.g., Humphreys (1978), Elias et al. (1985), Kleinmann & Hall (1986), Jura & Kleinmann (1990), Caron et al. (2003), Levesque et al. (2005), Figer et al. (2006), Davies et al. (2008), and Verhoelst et al. (2009). We also made use of the recent Galactic spectroscopic catalogs of bright late-type stars by Blum et al. (2003), Comerón et al. (2004), Clark et al. (2009), Liermann et al. (2009), Rayner et al. (2009),

---

[3] Version retrieved from CDS in November 2016.

Negueruela et al. (2010, 2011), Verheyen et al. (2012), Dorda et al. (2016), Messineo et al. (2017), and Dorda et al. (2018). Sources with available spectral types and good parallaxes (see Section 2.2) are listed in Table 1. For sources listed in these recent catalogs, spectral classifications provided in the corresponding papers have been retained (see footnotes to Table 1). The catalog by Skiff (2014) collected spectroscopic classifications of Galactic stars available from the literature, with some entries dating back to 1930–1950. For each star, one to a dozen entries were available. For stars for which only one reference is given (that to Skiff's database) we listed a spectral type range as well as the adopted spectral type, which is the mean (or most recent) of the measured spectral types.

2.2. Available Parallaxes

Gaia data were taken from the recently released *Gaia* DR2 catalog (Gaia Collaboration et al. 2016, 2018), which contains 1.7 billion sources. Typically, for parallaxes of stars brighter than $G = 14$ mag, quoted uncertainties are about 0.04 mas, ≈ 0.1 mas for $G = 17$ mag, and ≈ 0.7 mas for $G = 20$ mag (see Luri et al. 2018). Luminous late-type stars are characterized by brightness fluctuations due to convective motions and pulsation. The photocenters do not correspond to the stellar barycenters, but fluctuate around it (e.g., Chiavassa et al. 2011; Pasquato et al. 2011). This motion in general does not lead to systematic parallax errors; however, it degrades the goodness of fit of the astrometric solution (Chiavassa et al. 2011).

Initial celestial positions were taken from the catalog of Skiff (2014) and SIMBAD (Cambrésy et al. 2011) and improved with the positions of available Two Micron All Sky Survey (2MASS) matches. *Gaia* matches were searched using a radius of 1″.5. This resulted in 1342 *Gaia* sources, providing matches for 96% of the initial sample of late-type stars.

For 7.5% of the sample, parallaxes were available from both the *Gaia* DR2 and *Hipparcos* catalogs (ESA 1997); the mean difference of parallaxes is 0.08 mas, with a dispersion around the mean of 1.21 mas for stars with *Gaia* parallaxes larger than 2 mas.

2.2.1. Astrometric Quality Filtering and the Best Sample

The goal of this work is to build a catalog of secure known K-M stars of class I candidate RSGs in *Gaia* DR2, and therefore to derive their average absolute magnitude for each spectral type. This means that here we calculate the luminosity of the candidate RSGs by direct integration of their stellar energy distribution (SED), independently of colors or other information that might be obtained from the spectral energy distribution. Hence, we rely on the *Gaia* DR2 parallax only to estimate the distances of the sources in our sample. In order to make sure the corresponding luminosity estimates are robust we will apply a rather conservative filtering on the quality of the parallax data, as described in the following.

Throughout the text we indicate with σ_ϖ the external error of the parallax,[4] which is defined as $\sigma_\varpi(\text{ext}) = \sqrt{k^2 \times \sigma_\varpi(\text{int})^2 + \sigma_s^2}$, where $\sigma_\varpi(\text{int})$ is the internal error provided by DR2, $k = 1.08$ and $\sigma_s = 0.021$ mas for $G < 13$ mag (bright), and $k = 1.08$ and $\sigma_s = 0.043$ mas for $G \gtrsim 13$ (faint).
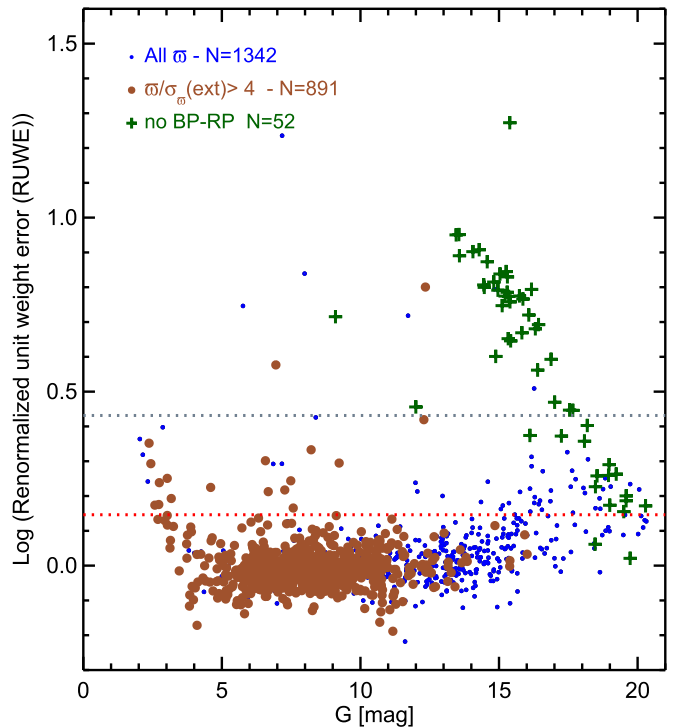
Figure 1. Value of the RUWE vs. the apparent brightness in G for all the sources in our sample. The two lines indicate the limits RUWE = 1.4 (in red) and RUWE = 2.7 (in gray). The large brown dots indicate stars for which $\varpi/\sigma_\varpi(\text{ext}) > 4$, while the dark green crosses indicate stars for which no color information is available from *Gaia* DR2.

In order to select sources with good quality astrometry we analyzed the ϖ/σ_ϖ ratio and the so-called renormalized unit weight error (RUWE) which the *Gaia* team recommends using instead of the filtering on the unit weight error described in Appendix C of Lindegren et al. (2018). The RUWE can be calculated using lookup tables available from the ESA *Gaia* webpages (see footnote 3) and it is described in detail in a publicly available technical note (Lindegren et al. 2018). In Figure 1 we show the RUWE as a function of G for all the sources in our sample.

Stars for which $\varpi/\sigma_\varpi > 4$ are indicated separately, as well as stars for which no color information is available (for which the value of the RUWE is less certain, this concerns 52 out of the 1342 sources in the sample). From this figure it is clear that most sources for which $\varpi/\sigma_\varpi > 4$ have a RUWE value below 1.4 (the threshold value recommended in Lindegren et al. 2018). A few stars with high signal-to-noise parallax values are located at $1.4 < \text{RUWE} < 2.7$. This suggests that a more relaxed filtering at RUWE < 2.7 is adequate for RSGs, so as to retain the brightest stars for which the RUWE values may be affected by photocenter motions.

We further restricted our sample to stars with $\varpi/\sigma_\varpi > 4$ in order to ensure robust distance estimates. We explain this in the next section. In the end, we thus retained 889 sources with $\varpi/\sigma_\varpi > 4$ and RUWE < 2.7. The parallax range of the sources after filtering is 0.19–7.53 mas.

2.3. Distance Estimates

The proper use of parallaxes in the distance estimation problem has been extensively reviewed in the context of *Gaia* DR2 by Luri et al. (2018). Their recommendation is not to use

---

[4] https://www.cosmos.esa.int/web/gaia/dr2-known-issues
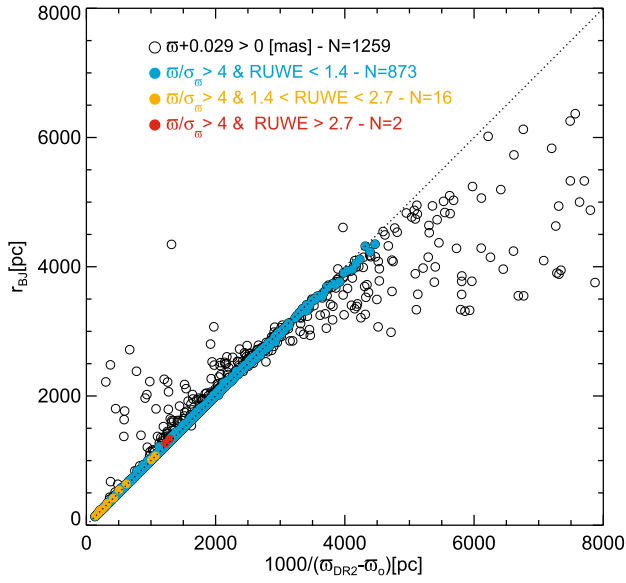
Figure 2. *Gaia* data. Parallactic distances inferred with the Milky Way model by Bailer-Jones et al. (2018) vs. parallactic distances from direct inversion of the parallaxes. The filled dots mark data points with ϖ/σ_ϖ(ext) > 4; in cyan: RUWE < 1.4; in orange: 1.4 < RUWE $\lesssim$ 2.7; and in red: RUWE > 2.7. The dotted line shows the points of the equation $r_{BJ} - (1000/(\varpi - \varpi_o)) = 0$ pc.

the inverse of the parallax as a distance indicator but to combine the parallax with other information and treat the estimation of distance as an inference problem. In our case we wish to use only the parallax in order to establish the luminosity of our stars independent from other information and in that case the Bayesian distance estimation method proposed by Bailer-Jones (2015), in particular using the exponentially decreasing space density prior, is a good choice (Luri et al. 2018). We will use the distances estimated by Bailer-Jones et al. (2018) for our selection of source with good quality and precise parallaxes, for the following reasons. For parallaxes with ϖ/σ_ϖ(ext) > 4 the Bailer-Jones et al. (2018) distances by design give essentially the same result as the $1/\varpi$ estimator, because for any reasonable length scale, L, of the exponentially decreasing space density prior, the likelihood dominates the posterior on the distances. At larger relative parallax error, the prior plays a stronger role, which would make our luminosity class estimates somewhat dependent on the Galactic model employed as a prior by Bailer-Jones et al. (2018). We verified that for our sources the relative differences between the $1/(\varpi - \varpi_0)$[5] and Bailer-Jones et al. (2018) distance estimates are less than 5% (see Figure 2), with no trends as a function of the value of L. A summary of relative differences between the $1/(\varpi - \varpi_0)$ and the Bailer's distances (R_{BJ}) is provided in Table 2.

Using the distance estimates from Bailer-Jones et al. (2018) even for our sample with very precise parallaxes has the added advantage that the uncertainties on the distance estimates (as well as on the distance moduli used below) are well defined. On the contrary, the $1/\varpi$ distance estimator follows a probability distribution that cannot be normalized and thus has no expectation value or variance. Parallax uncertainties propagated into distance uncertainties ($\sigma_d \approx \sigma_\varpi/\varpi^2$) are thus

formally meaningless for the $1/\varpi$ distance estimator (see Luri et al. 2018).

2.3.1. RSGs Related to Clusters and Radio Parallaxes

In this work, we treated the stars individually. However, in Table 1 we have annotated possible associations with known clusters, which is based on current literature. Only 13% of the sample was found to be associated. Memberships are not the focus of this work as they require an extensive and careful revision of each open cluster. For example, with *Gaia* DR2 data doubt is cast even upon the association of η Car with the young cluster Trumpler 16 (Davidson et al. 2018).

The 22 RSGs reported in Table 1 as being associated with the Per OB1 association yield an average $\varpi + 0.029 = 0.51$ mas with a dispersion around the mean of 0.13 mas, or an average $\varpi + 0.029 = 0.54$ mas with a dispersion of 0.11 mas when including only the best-quality sources. The annual parallax of maser spots measured toward S Persei is 0.413 ± 0.017 mas (Asaki et al. 2010). Unfortunately, the *Gaia* parallax of S Persei ($G = 7.80$ mag) has a large uncertainty, $\varpi = 0.22 \pm 0.13$ mas, RUWE = 1.27, ϖ/σ_ϖ(ext) = 1.67. Zhang et al. (2012) and Choi et al. (2008) reported on astrometric observations of H_2O masers around the RSG VY Canis Majoris ($G = 7.17$ mag). The trigonometric parallax is 0.88 ± 0.08 mas, corresponding to a distance of $1.14^{0.11}_{-0.09}$ kpc. Unfortunately, *Gaia* measurements are highly uncertain ($\varpi < -5.92 \pm 0.89$ mas, RUWE = 17.19).

The red hypergiant VX Sgr ($G = 7.17$ mag) has a trigonometric parallax of 0.64 ± 0.04 mas, corresponding to a distance of $1.56^{+0.11}_{-0.10}$ kpc (via water maser observations, Xu et al. 2018). Chen et al. (2007) estimated a distance of 1.57 ± 0.27 kpc with SiO maser observations. The *Gaia* parallax is $\varpi = 0.79 \pm 0.27$ mas, $1.36^{+1.02}_{-0.41}$ kpc (RUWE = 1.96, ϖ/σ_ϖ(ext) = 3.17). VX Sgr remains outside our selected 889 stars because of its low ϖ/σ_ϖ; however, the radio parallax and *Gaia* parallax agree within 23%.

The RSG PZ Cas ($G = 6.64$ mag) has an annual parallax of 0.356 ± 0.026 mas, corresponding to a distance of $2.81^{+0.22}_{-0.19}$ kpc (from water maser observations, Kusuno et al. 2013). *Gaia* measurements are consistent within errors ($\varpi = 0.42 \pm 0.09$ mas, $2.22^{+0.53}_{-0.36}$ kpc, RUWE = 1.06, ϖ/σ_ϖ(ext) = 4.67). PZ Cas is listed in Table 1. The radio and *Gaia* parallaxes agree within 18%.

2.4. Photometric Catalog

Photometric JHK_s measurements from the 2MASS catalog (Cutri et al. 2003; Skrutskie et al. 2006) were available for 97% of the sample in Table 1. Their K_s values range from -4 mag to about 12.5 mag. Of the K_s magnitudes, 43% are brighter than $K_s = 4$ mag, and magnitudes are based on the fitting of the wing of the PSF on the 51 ms exposures (red flag Rk = 3, see Table 1). For 6.5% of these stars, we were also able to retrieve J, H, and K measurements in the Catalog of Infrared Observations, CIO 5th edition, by Gezari et al. (1996); the average difference at 2 μm is 0.13 mag with $\sigma = 0.14$ mag. For the remaining 2.7% of the sample with missing near-infrared measurements, we used the photometry of Morel & Magnenat (1978), Liermann et al. (2009), Messineo et al. (2010), and Stolte et al. (2015). For the faintest star OGLE BW3 V 93508 ($K = 13.9$ mag) the measurements are from Lucas et al. (2008).

---

[5] $\varpi_0 = -0.029$ mas is the parallax zero-point estimated by Lindegren et al. (2018).

Table 1
Parallaxes and Spectral Types of the 889 Stars with $\varpi/\sigma_\varpi > 4$ and RUWE < 2.7

				Gaia							Sptype		Distance		Cluster
Id	Alias	R.A.(J2000)	Decl.(J2000)	ID	ϖ	pmRa	pmDec	G	Vel[a]	Sp (Skiff)	Sp(adopt)	Ref	Inv	MW	
		[hh mm ss]	[dd mm ss]		(mas)	(mas yr^{-1})	(mas yr^{-1})	(mag)	(km s^{-1})				(pc)	(pc)	
1	PER002	0:00:18.123	60:21:01.538	423337510285997440	1.32 ± 0.07	−6.831 ± 0.081	−1.540 ± 0.089	6.784 ± 0.002	⋯	⋯	M4.5 Ib	4	743	744^{+33}_{-31}	⋯
2	PER006	0:02:59.105	61:22:05.344	429500547840721536	0.98 ± 0.04	−1.181 ± 0.059	−1.221 ± 0.056	8.490 ± 0.001	−45.580 ± 0.190	⋯	M3 Ib	4	990	992^{+36}_{-34}	⋯
3	PER008	0:06:38.571	58:02:18.208	422677631507971840	0.82 ± 0.08	−3.328 ± 0.099	−3.282 ± 0.089	9.598 ± 0.002	⋯	⋯	M5 Ib	4	1176	1183^{+117}_{-98}	⋯
4	PER010	0:09:26.327	63:57:14.090	431678852171577216	0.40 ± 0.07	−3.633 ± 0.098	−0.372 ± 0.110	6.768 ± 0.012	−54.300 ± 0.530	⋯	M2 Iab	4	2350	2355^{+423}_{-314}	⋯
5	KN *Cas*	0:09:36.363	62:40:04.091	429999760479435520	0.29 ± 0.06	−1.850 ± 0.077	−1.817 ± 0.059	8.356 ± 0.002	⋯	⋯	M1 Ib	1, 5, 9	3131	3082^{+558}_{-416}	Cas OB5
6	PER012	0:12:21.655	62:53:33.738	431331097263392384	0.95 ± 0.04	−1.455 ± 0.043	−2.351 ± 0.044	6.914 ± 0.000	−35.120 ± 0.150	⋯	K0 Iab	1,4	1025	1026^{+29}_{-27}	⋯
7	PER015	0:15:01.100	66:06:50.122	528168213046737024	2.16 ± 0.04	5.334 ± 0.048	−5.527 ± 0.046	7.231 ± 0.001	−32.050 ± 0.180	⋯	K3 Ib	4	456	456^{+7}_{-7}	⋯
8	PER019	0:18:26.380	60:54:09.149	428817510598195584	0.42 ± 0.04	−2.826 ± 0.049	−1.200 ± 0.044	7.795 ± 0.001	−49.280 ± 0.170	⋯	M1 Iab	4	2222	2220^{+165}_{-144}	⋯
9	PER022	0:20:43.560	61:52:46.537	430464235421496320	0.81 ± 0.09	−1.599 ± 0.104	−0.334 ± 0.094	5.760 ± 0.002	−29.740 ± 0.320	⋯	M1 Iab	4,8	1188	1198^{+130}_{-107}	⋯
10	BD + 59 38	0:21:24.278	59:57:11.155	428379733171150336	0.53 ± 0.07	−3.470 ± 0.084	−0.924 ± 0.070	7.966 ± 0.005	−55.570 ± 0.850	⋯	M2/M2 Iab/I	1, 2, 5, 8, 9	1778	1783^{+230}_{-184}	Cas OB4

Notes. The identification number (Id) is followed by an Alias name, the *Gaia* coordinates, the *Gaia* parameters (name = ID, parallax = ϖ and its external error (σ_ϖ), proper motions, *G*-band magnitude, Vel), the spectral types (Sp(Skiff)) collected by Skiff (2014), the adopted spectral type (Sp(adopt)), references for the spectral types (Ref), distances, and nearby clusters. Sp(adopt) is that of the first reference listed, which is ≠1. When only Skiff's reference is present (=1), an average spectral type from Skiff's records is adopted and the encountered spectral range is annotated (Sp(Skiff)). When Levesque et al.'s (2005) reference is present (=2), two values are provided, the photographic MK type and class, and the new type by Levesque et al. (2005) (revised by fitting synthetic models). "Inv" distances are obtained by inversion of the parallaxes; "MW" distances and relative errors are those of Bailer-Jones et al. (2018), and are based on a prior derived from a Milky Way model. Extra notes based on checks and private communication with Skiff during the printing of this manuscript: CD-57 3502 is a wrong alias in Elias et al. (1985), with the entry can be ignored. The correct star is CPD -57 3502 (B. A. Skiff 2019, private communication). HD 142686 is wrong alias in Humphreys et al. (1978), and the entry can be ignored. The correct star is HD 142696 (B. A. Skiff 2019, private communication). CPD-59 4549 is wrong alias in Humphreys et al. (1978), and the entry can be ignored. The correct star is CD-59 4459 (B. A. Skiff 2019, private communication). Due to a format issue, some classes from Dorda et al. (2018) are not correct (e.g., Ib-II is truncate as Ib). This does not affect the results. See also https://somethingaboutrsgstars.wordpress.com/errata.
[a] Spectroscopic radial velocity in the solar barycentric reference frame.

References: (2) Levesque et al. (2005), (3) Verhoelst et al. (2009), (4) Dorda et al. (2018), (5) Dorda et al. (2016), (6) Kleinmann & Hall (1986), (7) Elias et al. (1985), (8) Jura & Kleinmann (1990), (9) Humphreys (1978), (10) Messineo et al. (2017), (11) Messineo et al. (2014), (12) Negueruela et al. (2012), (13) Negueruela et al. (2011), (14) Rayner et al. (2009), (15) Liermann et al. (2009), (16) Mermilliod et al. (2008), (17) Messineo et al. (2008), (18) Mengel & Tacconi-Garman (2007), (19) Caron et al. (2003), (20) Massey et al. (2001), (21) Eggenberger et al. (2002).

(This table is available in its entirety in machine-readable form.)

Table 2
Average Difference of the Distances Provided by Bailer-Jones et al. (2018), $\langle R_{BJ}\rangle$ and Distances from Direct Inversion of the Parallaxes for Stars with $\varpi/\sigma_\varpi(\text{ext}) > 2$, 3, 4, 5, and 10

ϖ/σ_ϖ	N_{stars}	All						dist > 3.5 kpc					
		$\Delta(\text{dist})$ (pc)	σ (pc)	$\langle\Delta(\text{M1})\rangle$ (mag)	σ (mag)	$\langle\Delta(\text{M2})\rangle$ (mag)	σ (mag)	$\Delta(\text{dist})$ (pc)	σ (pc)	$\langle\Delta(\text{M1})\rangle$ (mag)	σ (mag)	$\langle\Delta(\text{M2})\rangle$ (mag)	σ (mag)
2	1075	−5.58	123.74	0.017	0.093	0.63	0.56	−289.04	316.95	−0.13	0.11	0.96	0.25
3	981	2.78	44.44	0.014	0.045	0.51	0.38	−124.94	105.35	−0.06	0.04	0.82	0.18
4	**891**	**3.98**	**22.42**	**0.011**	**0.026**	**0.45**	**0.25**	**−83.72**	**47.32**	**−0.05**	**0.03**	**0.70**	**0.08**
5	805	5.22	13.13	0.01	0.02	0.39	0.20	−58.394	23.28	−0.03	0.01	0.62	0.01
10	379	2.92	2.59	0.006	0.007	0.21	0.10	⋯	⋯				

Note. $\Delta(\text{dist}) = \langle R_{BJ} - 1000/(\varpi - \varpi_0)\rangle$. $\langle\Delta(\text{M1})\rangle$ is the difference in the distance moduli inferred with the two distances $\langle R_{BJ}\rangle$ and $\langle 1000/(\varpi - \varpi_0)\rangle$. $\langle\Delta(\text{M2})\rangle$ is the difference in the distance moduli of the high and low distances inferred by Bailer-Jones et al. (2018). The line in bold indicates the value of ϖ/σ_ϖ at which $\langle\Delta(\text{M1})\rangle$ is always less than 5%.

For 78% of the stars, mid-infrared measurements from the *Midcourse Space Experiment* (*MSX*, Price et al. 2001; Egan et al. 2003) were available. For 27% of the sample, 24 μm measurements from MIPSGAL by Gutermuth & Heyer (2015) were available. For 32% of the sample, there were GLIMPSE measurements (Benjamin et al. 2005; Churchwell et al. 2009); for 96%, mid-infrared measurements from 3.6 to 22 μm were available from the *Wide-field Infrared Survey Explorer* (*WISE*) (Wright et al. 2010). We used an initial search radius of 5″ and selected the closest matches. The *MSX* matches were at an average distance of 1″3 with $\sigma = 0″9$ from the 2MASS positions; the *WISE* matches at an average distance of 0″4 ($\sigma = 0″4$). The *Gaia* positions were searched to within 1″5 of the 2MASS positions, and have an average displacement of 0″17 and a $\sigma = 0″13$ from the 2MASS centroids; 2MASS stars are the closest matches to the *Gaia* sources and also the brightest K_s sources. Matches were confirmed with a visual inspection of 2MASS and *WISE* images, as well as of the SED. Notes on the matches are provided in the Appendix.

BVR photometry was retrieved from The Naval Observatory Merged Astrometric Dataset (NOMAD) (Zacharias et al. 2005). The photometric data for the subsample of 889 stars with good parallaxes are listed in Table 3.

3. Luminosities

3.1. Bolometric Magnitudes

We estimated the stellar luminosities using the photometric measurements, an extinction power law with an index of 1.9 (Messineo et al. 2005), and the distance moduli derived from the *Gaia* parallaxes. For spectral types from K0 to M5, intrinsic $J-K_s$ and $H-K_s$ colors were taken from Koornneef (1983). For M6–M9 types, intrinsic colors were derived from the colors of giants (e.g., Koornneef 1983; Montegriffo et al. 1998; Cordier et al. 2007), and the average offset between the colors of giants and supergiants of types M3–M5 were applied. Bolometric corrections to the absolute K-magnitudes were provided by Levesque et al. (2005). In addition to this calculation, we performed a direct flux integration using the JHK_s measurements, and the mid-infrared measurements from *MSX*, *WISE*, GLIMPSE, and MIPSGAL. Measurements were dereddened with extinction ratios as described in Messineo et al. (2005). The integral under the SED was estimated with the trapezium method; flux extrapolations at the red extremes were performed with a linear interpolation passing through the last reddest data point and going to zero flux at 500 μm, while for those at the

blue extreme (bluer than *J*-band) we used a blackbody extrapolation (see Messineo et al. 2017). Red extrapolation contains about 5‰ of the flux. The average difference between the M_{bol} calculated with the BC_{K_s} and those calculated by integrating under the SED is 0.05 mag, with a $\sigma = 0.18$ mag. Inferred M_{bol} values are listed in Table 4.

We estimated dereddened *BV* photometry, V_o and B_o, using the estimated A_{K_s} and assuming $R = 3.1$ and the extinction ratios in Messineo et al. (2005).

3.2. Luminosity Classes and Nuclear Burnings

The MK system was established in 1943 by Morgan and Keenan, and it is an empirical system for the stellar spectral classification. It is based on a known atlas of standard stars with spectral types and luminosity classes (Morgan et al. 1943). Stellar spectra are classified by direct comparison with spectra of standard stars observed at the same resolution and with the same instrument. Through quantitative spectral analysis one can estimate gravity, g, or T_{eff}; however, such quantities are external to the definition of MK system itself. While spectroscopic indicators of luminosity for dwarfs and evolved late-type stars are at our disposal from atomic lines and molecular bands, the separation of giants and supergiants remains difficult. Furthermore, spectroscopic optical and infrared classifications may provide somewhat different results (Gray & Corbally 2009); supplementary information on distances, luminosities, and chemical composition is necessary.

Higher extinction renders the M_V versus $B_o - V_o$ unsuitable for studies of the inner Galaxy, and it is useful to translate the optical quantities into infrared quantities and theoretical quantities. Furthermore, it is useful to look at these diagrams by keeping in mind which types of nuclear burnings may occur.

AGBs and RSGs are cold objects with similar ranges of effective temperatures, and therefore spectral types. They overlap in luminosity. AGB stars can even be brighter than RSGs, and it is not known a priori from the luminosity classes the type of internal nuclear burnings or their distances.

AGB stars are stars of low or intermediate masses ($\lesssim 9\,M_\odot$) burning helium and hydrogen in shells, with a degenerate core of CO. AGB stars from 6.5 to 9.5 $M_\odot$ experience off-center nuclear burnings and from 9 to 10 $M_\odot$ can even reach an iron core state and evolve into neutron stars.

As Iben (1974) writes, massive stars are stars that do not develop a strongly electron-degenerate core until all exoergic reactions have run to completion at the center. RSGs are massive stars from ≈ 9 to $\approx 40\,M_\odot$ (Ekström et al. 2012). Most

Table 3
Infrared Measurements of the Bright Late-type Stars in Table 1

ID	2MASS[a]									CIO			GLIMPSE				MSX				WISE				MIPS	NOMAD			Nstar[b]
	J	Rj	Qj	H	Rh	Qh	K_S	Rk	Qk	J	H	K	[3.6]	[4.5]	[5.8]	[8.0]	A	C	D	E	W1	W2	W3	W4	[24]	B	V	R	
	1.2			1.6			2.2			1.25	1.65	2.20	3.6	4.5	5.8	8.0	8.3	12.1	14.6	21.3	3.4	4.6	11.6	22.1	23.7				
	(mag)			(mag)			(mag)			(mag)	(mag)	(mag)	(mag)	(mag)	(mag)	(mag)	(mag)	(mag)	(mag)	(mag)	(mag)	(mag)	(mag)	(mag)	(mag)	(mag)	(mag)	(mag)	
1	3.56	3	D	2.64	3	C	2.18	3	D	...	...	...	...	...	...	...	1.87	1.86	1.62	...	...	...	1.97	1.79	...	10.15	8.48	7.60	110
2	5.53	1	A	4.62	1	A	4.30	1	A	...	...	...	...	...	...	...	4.17	...	...	...	4.19	4.05	4.21	4.06	...	11.49	9.75	8.87	110
3	5.81	1	A	4.86	1	E	4.48	1	A	...	...	...	...	...	...	...	4.30	...	...	...	4.37	4.32	4.29	4.11	...	16.46	...	10.50	110
4	3.21	3	D	2.15	3	D	1.73	3	D	...	...	1.81	...	...	...	...	0.17	−0.42	−0.39	−1.18	...	...	−0.23	−1.22	...	10.22	8.37	7.49	110
5	5.25	1	A	4.53	3	D	4.29	3	D	...	...	...	...	...	...	...	3.74	3.60	...	...	3.80	3.68	3.73	3.53	...	11.30	9.57	8.69	110
6	5.03	3	D	4.08	3	D	3.64	1	E	...	...	...	...	...	...	...	3.48	3.44	...	...	3.53	3.40	3.55	3.47	...	9.25	7.55	6.67	110
7	4.53	3	D	3.66	3	C	3.36	3	D	...	...	...	...	...	...	...	3.27	3.39	...	...	...	3.25	3.34	3.23	...	10.11	8.20	7.32	110
8	4.79	3	D	3.74	3	D	3.25	3	D	...	...	...	...	...	...	...	2.98	2.77	2.69	...	...	3.06	2.99	2.60	...	11.41	9.10	8.53	110
9	3.12	3	D	2.26	3	C	1.88	3	D	...	...	1.75	...	...	...	...	1.53	1.44	1.37	1.45	...	...	1.65	1.48	...	8.82	6.85	5.97	110
10	4.58	3	D	3.43	3	D	2.71	3	D	...	...	...	...	...	...	...	0.97	0.28	0.45	−0.12	...	...	0.50	−0.12	...	11.82	9.66	8.94	110

Notes. The identification number (Id) is followed by the 2MASS *JHK* measurements with corresponding red flags (Rj, Rh, Rk) and quality flags (Qj, Qh, Qk), CIO *JHK* magnitudes, *MSX A*, *C*, *D*, *E* magnitudes, *WISE W*1, *W*2, *W*3, *W*4 magnitudes, MIPS 24 μm magnitude, the NOMAD *BVR* magnitudes, and the Nstar value. A few *WISE* and *MSX* measurements were discarded (see the Appendix).
[a] If the 2MASS quality flags are equal to "M" the measurements have other origins specified in the Appendix.
[b] Nstar = XYZ, where X = number of *MSX* detected within the search radius; Y = number of *WISE* stars within the search radius; and Z = number of GLIMPSE stars with 8 μm magnitudes <10 within the search radius. A value of 9 indicates that the counter is not available.

(This table is available in its entirety in machine-readable form.)

Table 4
Properties of Bright Late-type Stars from Table 1

Id	Sp.Type	Class(adopt)	Area	$T_{\rm eff}$	J–$K_{\rm s}$	H–$K_{\rm s}$	$A_{K_{\rm s}}(JK)$	$A_{K_{\rm s}}(HK)$	$BC_{K_{\rm s}}$[a]	$K_{\rm so}$[b]	$M_{\rm bol}$[c]	$M_{\rm bol2}$[d]	DM[e]	Mbol-Q[f]	V_o	R
				(K)	(mag)	(mag)	(mag)	(mag)	(mag)	(mag)	(mag)	(mag)	(mag)		(mag)	($R_\odot$)
1	M4.5	Ib	E	3535.00 ± 170.00	1.25	0.30	0.07 ± 0.19	0.24 ± 0.47	2.89	2.11 ± 0.31	$-4.35^{-0.33}_{+0.32}$	$-4.24^{-0.26}_{+0.25}$	$9.36^{-0.10}_{+0.09}$	2	7.88	175
2	M3	Ib	F	3605.00 ± 170.00	1.16	0.28	0.03 ± 0.01	0.06 ± 0.03	2.84	4.27 ± 0.02	$-2.87^{-0.10}_{+0.10}$	$-2.76^{-0.09}_{+0.09}$	$9.98^{-0.08}_{+0.08}$	2	9.45	85
3	M5	Ib	F	3450.00 ± 170.00	1.30	0.32	0.01 ± 0.01	0.09 ± 0.06	2.96	4.47 ± 0.02	$-2.94^{-0.22}_{+0.20}$	$-2.83^{-0.21}_{+0.20}$	$10.36^{-0.21}_{+0.19}$	1	…	96
4	M2	Iab	A	3660.00 ± 170.00	1.06	0.25	0.22 ± 0.18	0.24 ± 0.48	2.80	1.51 ± 0.29	$-7.55^{-0.47}_{+0.43}$	$-7.54^{-0.42}_{+0.38}$	$11.86^{-0.36}_{+0.31}$	2	6.39	716
5	M1	Ib	B	3745.00 ± 170.00	1.00	0.22	−0.02 ± 0.22	0.03 ± 0.70	2.73	4.29 ± 0.46	$-5.42^{-0.59}_{+0.56}$	$-5.35^{-0.39}_{+0.36}$	$12.44^{-0.36}_{+0.32}$	2	9.57	256
6	K0	Iab	D	4185.00 ± 85.00	0.58	0.12	0.43 ± 0.15	0.46 ± 0.40	2.40	3.21 ± 0.15	$-4.45^{-0.17}_{+0.17}$	$-4.36^{-0.25}_{+0.25}$	$10.06^{-0.06}_{+0.06}$	1	3.68	131
7	K3	Ib	F	3985.83 ± 170.00	0.72	0.15	0.24 ± 0.18	0.23 ± 0.44	2.55	3.11 ± 0.29	$-2.63^{-0.30}_{+0.30}$	$-2.58^{-0.23}_{+0.23}$	$8.30^{-0.03}_{+0.03}$	2	6.02	62
8	M1	Iab	B	3745.00 ± 170.00	1.00	0.22	0.29 ± 0.21	0.40 ± 0.58	2.73	2.97 ± 0.37	$-6.03^{-0.41}_{+0.41}$	$-5.93^{-0.29}_{+0.29}$	$11.73^{-0.16}_{+0.15}$	2	6.53	339
9	M1	Iab	B	3745.00 ± 170.00	1.00	0.22	0.13 ± 0.18	0.24 ± 0.43	2.73	1.75 ± 0.28	$-5.91^{-0.36}_{+0.35}$	$-5.82^{-0.31}_{+0.30}$	$10.39^{-0.22}_{+0.20}$	2	5.70	321
10	M2	I	B	3660.00 ± 170.00	1.06	0.25	0.43 ± 0.23	0.70 ± 0.55	2.80	2.27 ± 0.37	$-6.18^{-0.46}_{+0.44}$	$-6.15^{-0.37}_{+0.36}$	$11.26^{-0.26}_{+0.24}$	2	5.78	381

Notes. The identification number (Id) from Table 1 is followed by the spectral type and class adopted from the literature, Sp(adopt) and Class(adopt), by the area occupied in the $M_{\rm bol}$ versus $T_{\rm eff}$ plot (Area), the $T_{\rm eff}$ value, the intrinsic J–$K_{\rm s}$ and H–$K_{\rm s}$ colors, the extinction $A_{K_{\rm s}}(JK)$ and $A_{K_{\rm s}}(HK)$ derived from the JK and HK colors, the adopted $BC_{K_{\rm s}}$, the dereddened $K_{\rm s}$, $K_{\rm so}$, two estimates of bolometric magnitudes, the DM obtained with the distances of Bailer-Jones et al. (2018), a flag for best near-infrared photometry (Mbol-Q), the dereddened V magnitude, V_o, and the stellar radius (R) estimated with the equation of Josselin & Plez (2007). A few $A_{K_{\rm s}}$ values are negative. No extinction correction was applied for these stars.

[a] For BC_K, values are calculated with the formula of Levesque et al. (2005) and a typical error of 0.06 mag is assumed (average difference between the BC_K values of two spectral types).

[b] The errors on the $K_{\rm so}$ values are estimated by propagating the photometric errors and the $A_{K_{\rm s}}$ errors.

[c] The $M_{\rm bol}$ values are obtained with the BC_K; their errors are estimated by propagating the errors on $K_{\rm so}$, BC_K, and DMs.

[d] The $M_{\rm bol2}$ values are obtained via integration under the SED (see Section 3.1). Errors are estimated by lowering the curve by subtracting the photometric errors, and by lifting up the curve by adding the photometric curve. The DM error is then added by Taylor's propagation law.

[e] DM is here the distance module obtained with the Bailer distance. Its error is obtained using the quoted high and low values from Bailer-Jones et al. (2018).

[f] Mbol-Q is set to unity when $\varpi/\sigma_\varpi > 4$ and RUWE < 2.7 (889 sources), and set to 2 when $\varpi/\sigma_\varpi > 4$ and RUWE < 2.7 and $JHK_{\rm s}$ quality flags are A (2MASS) or B (2MASS) or C (2MASS) or D (2MASS) or M (HST photometry).

(This table is available in its entirety in machine-readable form.)

Table 5
Summary of M_{bol} and Temperatures of Galactic Massive Cool Stars (RSGs) and Other Cool Stars of Low and Intermediate Masses

Mass $M_\odot$	Age_to_red (Myr)	T_red (Myr)	Phase	M_{bol} (mag)	T_{eff} (K)	Sp. Type	Comments
0.6–0.8			tip-rgb	[−3.6, −3.8]			Observed range in globular clusters (Ferraro et al. 2000)
1.35–1.7			tip-rgb	[3.4]			Rot. tracks by Ekström et al. (2012)
<2.0 − 2.8			tip-rgb	[**−3.5, −3.7**]			He-flash theory **for Z = 0.01** (Sweigart et al. 1990)
			AGB-Mira	[−5.0, −7.1]			Observed bulge stars in Alard et al. (2001)
			AGB-Mira		<3500	M4–M9	Observed range in the Bulge (Blanco et al. 1984)
0.85[a]	11.8[a]		AGB-Mira		<3500	M4–M5	Observed range in old 47 Tuc (Glass & Feast 1973; Skiff 2014)
			AGB-SR	[−2.5, −5.0]			Observed. Bulge stars in Alard et al. (2001)
1	11250	12	AGB	[− 3.61, − 4.03]			M_{bol} during E-AGB and TP-AGB by Vassiliadis & Wood (1993)
2	1236	9	AGB	[− 3.78, − 4.90]			M_{bol} during E-AGB and TP-AGB by Vassiliadis & Wood (1993)
3.5	230	3	AGB	[− 5.17, − 5.65]			M_{bol} during E-AGB and TP-AGB by Vassiliadis & Wood (1993)
5	95	1.4	AGB	[− 5.91, − 6.22]			M_{bol} during E-AGB and TP-AGB by Vassiliadis & Wood (1993)
7			S-AGB	[−6.86]			minimum M_{bol}[b] Doherty et al. (2015)
8			S-AGB	[−7.20]			minimum M_{bol}[b] Doherty et al. (2015)
9			S-AGB	[−7.60]			minimum M_{bol}[b] Doherty et al. (2015)
9.8			S-AGB	[−7.86]			minimum M_{bol}[b] Doherty et al. (2015)
3	417		S-AGB	[−0.3, −1.7]	4850–4300	>K0	Rot. tracks[c] by Ekström et al. (2012)
5	111		S-AGB	[−2.3, −4.4]	4600–3800	>K0–M0	Rot. tracks[c] by Ekström et al. (2012)
7	52		S-AGB	[−3.5, −5.9]	4400–3550	>K0–M3.5	Rot. tracks[c] by Ekström et al. (2012)
9	32	3.7	RSG	[−4.5, −6.8]	4200–3500	K0–M4.5	Rot. tracks by Ekström et al. (2012)
12	20	2.0	RSG	[−6.0, −7.4]	3900–3550	K4–M3.5	Rot. tracks Ekström et al. (2012)
15	12.5	1.0	RSG	[−7.3, −7.9]	3750–3600	M1–M2	Rot. tracks Ekström et al. (2012)
20	9.9		RSG	[−8.2]	3774	M0.5	Rot. tracks Ekström et al. (2012)
25	8.0		RSG	[−8.79]	3836	K5	Rot. tracks Ekström et al. (2012)
			RSG	[−3.63, −10.36]			Observed range by Levesque et al. (2005)

Notes.
[a] Age of 47 Tuc (Brogaard et al. 2017).
[b] During the interpulse phase.
[c] Evolved up the early asymptotic giant branch.

of them are burning He when they reach the RSG phase. For an RSG of 9 $M_\odot$ models predict M_{bol} from −4.5 to −6.8 mag and spectral types from K0 to M4.5, while for an RSG of 25 $M_\odot$, models predict $M_{bol} \approx -8.8$ mag and spectral type K5 (see Table 5). Observations closely follow the new evolutionary tracks by Ekström et al. (2012). The M_{bol} values of the ≈90 Galactic RSGs recently analyzed by Levesque et al. (2005) range from $M_{bol} = -3.63$ mag to $M_{bol} = -10.36$ mag.

A few observational luminosity benchmarks of late-type stars of low and intermediate masses are useful here. The tip of red giant branch stars in Galactic globular clusters occurs at $M_{bol} = -3.6$ to −3.8 mag in metal-rich globular clusters, such us 47 Tuc (e.g., Ferraro et al. 2000); members brighter than that are thermally pulsing TP-AGBs. The maximum luminosity that more massive AGB stars can reach is about −7.1 mag (Vassiliadis & Wood 1993). Very massive AGB stars may experience hot-bottom burning, which further increases their luminosity, but this phenomenon primarily affects metal-poor populations and is thus expected to only moderately affect the Milky Way disk population. The latest models of Doherty et al. (2015) predict that a super-AGB of 9 $M_\odot$ would reach $M_{bol} < -7.6$ mag. Therefore, AGBs do have a large overlap in luminosity with RSGs, and may enter the luminosity classes

Ia, Ib, and Ib-II; for example, as pointed out by the kind referee, α Her is an AGB of 2–3 $M_\odot$ with class Ib-II (Moravveji et al. 2013), and NGC 6067 hosts several AGBs of 6 $M_\odot$ with types K0-K4 and classes Iab-Ib, Iab-Ib, and Ib (Alonso-Santiago et al. 2017).

However, observationally we can see that field AGB stars in the Baade's Windows with M_{bol} from ≈−5.0 to −7.1 mag are large-amplitude pulsators (Miras) (e.g., Alard et al. 2001), and generally have late-M spectral types, M4-M9 (i.e., T_{eff} cooler than 3500 K, Blanco et al. 1984; Alard et al. 2001); similarly, the 4 Mira stars (V1-V4) at the tip of the red branch of the globular cluster 47 Tuc have spectral types M4-M5 (Glass & Feast 1973; Skiff 2014). By contrast, semiregular AGB pulsators are typically fainter than Mira AGBs: $-2.5 \gtrsim M_{bol} \gtrsim -5.0$ mag, while Miras have $-3.6 \gtrsim M_{bol} \gtrsim -7$ mag (e.g., Alard et al. 2001).

In conclusion, only stars brighter than $M_{bol} \approx -7.5$ mag (masses >15 $M_\odot$) are certain RSGs; late-type stars earlier than M4 and with $M_{bol} \lesssim -5.0$ mag are expected to have masses $\gtrsim 5$–7 $M_\odot$. For field late-type stars fainter or redder than that, AGB stars are the dominant population when $M_{bol} < -3.6$ mag (see Table 5).
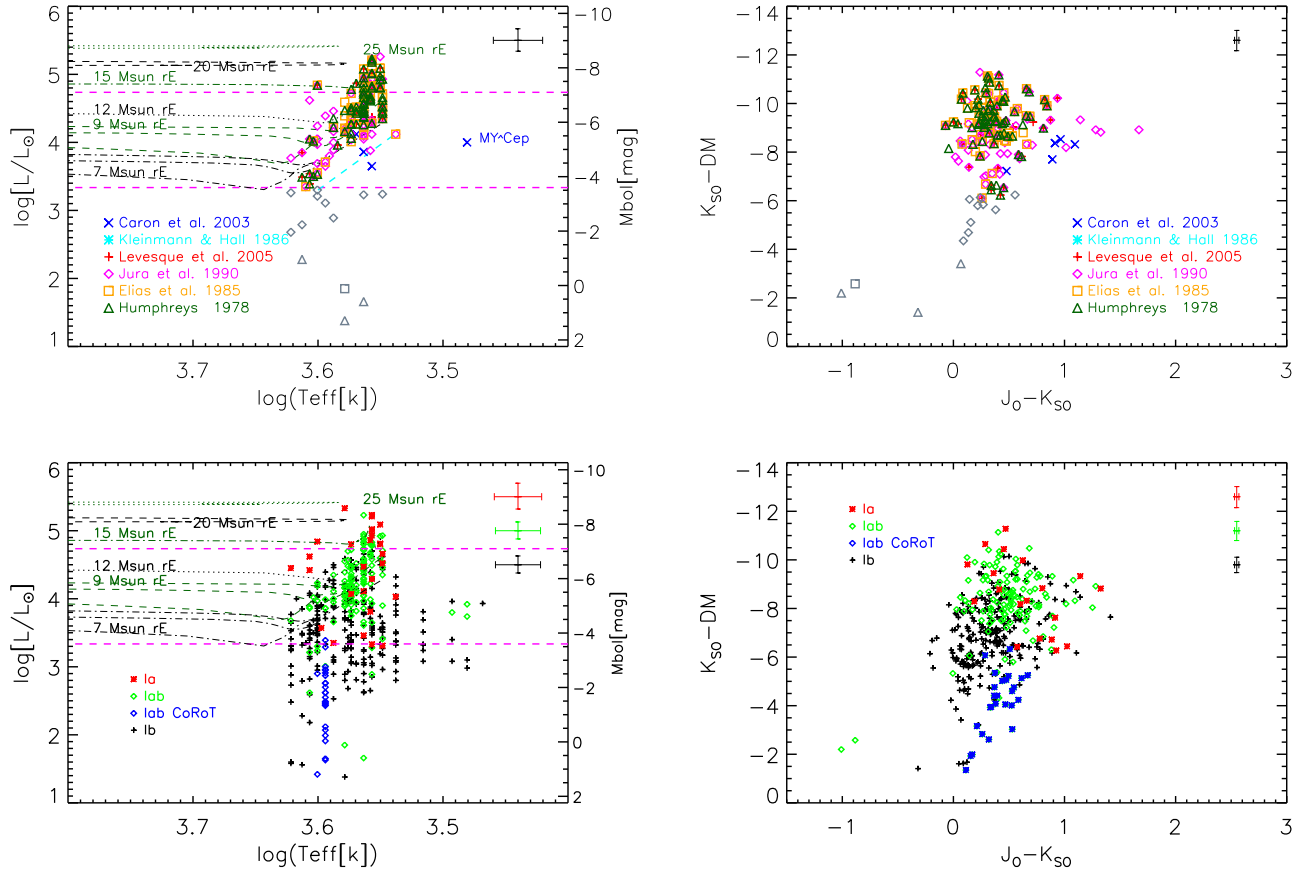
Figure 3. Top left panel: luminosities vs. $T_{\rm eff}$ values of reference RSGs (from class Ia to Ib), i.e., of the subsample of stars in Table 1 with given class I in the catalogs of Caron et al. (2003, blue crosses), Kleinmann & Hall (1986, cyan asterisck), Levesque et al. (2005, red pluses), Jura & Kleinmann (1990, magenta diamonds), Elias et al. (1985, orange squares), and Humphreys (1978, green triangles). An average error bar is drawn in the top right corner. The two magenta long-dashed horizontal lines mark $M_{\rm bol} = -3.6$ mag (tip of the red giant branch), and -7.1 mag (AGB limit). The long-dashed cyan line marks Equation (1); RSGs appear brighter and bluer than that locus (see the text). Stellar tracks from models at solar metallicity and including rotation are from Ekström et al. (2012); from the bottom to the top: the black dotted–dashed curve marks a stellar track of a $7\,M_\odot$ star; the green long-dashed curve marks a $9\,M_\odot$ track; the black dotted curve marks a $12\,M_\odot$ track; the green dotted–dashed curve shows a $15\,M_\odot$ track; the black long-dashed curve marks a $20\,M_\odot$ track; and the top green dotted line shows a $25\,M_\odot$ track. A few objects (in gray) remain fainter than the red giant tip (see the text). Top right panel: absolute and dereddened K_s magnitudes vs. dereddened $J-K_s$ colors. Data points are the same as described in the left panel. Bottom right panel: luminosities vs. $T_{\rm eff}$ values of stars in Table 1 with adopted class Ia, Iab, and Ib (stars detected by *CoRoT* and listed in Table 1 as class Iab should be regarded separately). Bottom left panel: absolute and dereddened K_s magnitudes vs. dereddened $J-K_s$ colors of stars in Table 1 with adopted class Ia, Iab, and Ib.

3.2.1. Reference RSGs

We consider as reference RSGs those stars included in the catalogs of Kleinmann & Hall (1986), Levesque et al. (2005), Caron et al. (2003), Jura & Kleinmann (1990), Elias et al. (1985), and Humphreys (1978). These sources are expected to be RSGs because they are located in the direction of OB associations. In the top left panel of Figure 3, we show their luminosities, $\log(L/L_\odot)$, versus $T_{\rm eff}$ (theoretical plane); in the bottom panel, we show their absolute and dereddened K_s, $K_{\rm so}-{\rm DM}$ versus $J_{\rm o} - K_{\rm so}$ (observational plane); DM is the distance moduli. By comparison with the stellar tracks, we estimated initial masses from about 7 to $25\,M_\odot$ (Ekström et al. 2012). Among them, the brightest star appears to be SW Cep with $M_{\rm bol} = -8.42$ mag. MY-Cep is the only M7.5 I included in the sample. A few stars were discarded as reference RSGs because they appeared too faint for luminosity class I ($M_{\rm bol} > -3.6$ mag, as shown in Figure 3); those stars are IRC+40105, 6 Aur, 1 Pup, sigOph, IRC +00328, 33 Sgr, 12 Peg, BD+47 3584, 56 Peg (Jura & Kleinmann 1990), CD-57 3502 (Elias et al. 1985), CPD-59 4549, HD 142686, and HD 150675 (Humphreys 1978).

3.2.2. Hertzsprung–Russell Diagram

All reference RSGs except for MY Cep appear to be located along the ascending stellar tracks in Figure 3. They are located to the left of the following equation (which is roughly parallel to the ascending parts of the tracks at the low $T_{\rm eff}$ end):

$$\log(L/L_\odot) = 51.3 - 13.33 \times \log(T_{\rm eff}), \qquad (1)$$

where $\log(T_{\rm eff})$ ranges from 3.54 to 3.6 (i.e., from M4 to K1, Levesque et al. 2005).

The temporal evolution of an AGB star is characterized by large excursion in the $M_{\rm bol}$ versus $T_{\rm eff}$ diagram. During the thermal pulses the luminosity increases and $T_{\rm eff}$ decreases. For example, a star of $3\,M_\odot$ may reach $M_{\rm bol} = \approx -2$ mag during the early-AGB phase and $M_{\rm bol} = \approx -5$ mag during thermal pulses (e.g., Vassiliadis & Wood 1993).

In Figure 4, we show the luminosities of stars in Table 4, and we verify their positions on the $M_{\rm bol}$ versus $T_{\rm eff}$ diagram using the described observational benchmarks and the features appearing in Figure 3:

(A) Area A contains late-type stars with $M_{\rm bol} \lesssim -7.1$ mag. They are expected to be mostly RSGs.
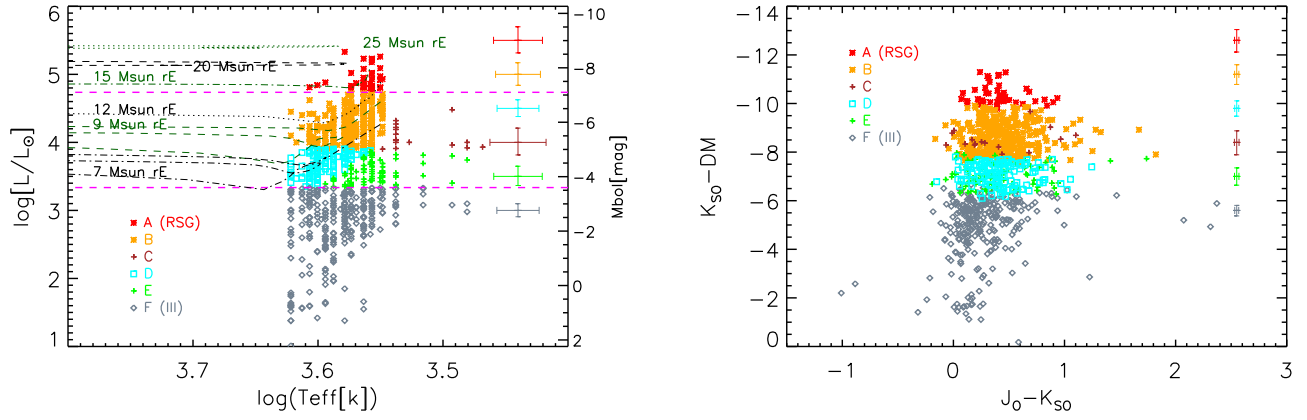
Figure 4. Left panel: luminosities vs. T_{eff} values of stars in Table 1 with $\varpi/\sigma_\varpi(ext) > 4$ and RUWE < 2.7. The red asterisks mark highly probable RSGs with $M_{bol} < -7.1$ mag (Area = A). The orange asterisks mark sources with $M_{bol} < -5.0$ mag and types $<M4$ (Area = B). The cyan squares mark sources with $-3.6 > M_{bol} > -5.0$ mag and that are bluer than Equation (1) (Area = D). The brown pluses ($M_{bol} < -5.0$ mag) and green pluses ($-3.6 > M_{bol} > -5.0$ mag) indicate Areas C and E. The gray diamonds indicate giants, i.e., stars fainter than $M_{bol} \approx -3.6$ (tip of the red giant branch, Area = F). The two magenta long-dashed horizontal lines mark $M_{bol} = -3.6$ mag (tip), mag, and $M_{bol} = -7.1$ mag (AGB limit). For comparison, we add some rotating stellar tracks with solar metallicity by Ekström et al. (2012). From the bottom to the top: the black dotted–dashed curve marks a stellar track of a 7 $M_\odot$ star; the green long-dashed curve marks a 9 $M_\odot$ track; the black dotted curve marks a 12 $M_\odot$ track; the green dotted–dashed curve shows a 15 $M_\odot$ track; the black long-dashed marks a 20 $M_\odot$ track; and the green dotted line shows a 25 $M_\odot$ track. Right panel: absolute and dereddened K_s magnitudes vs. dereddened $J-K_s$ colors. Data points are the same as those described in the left panel.
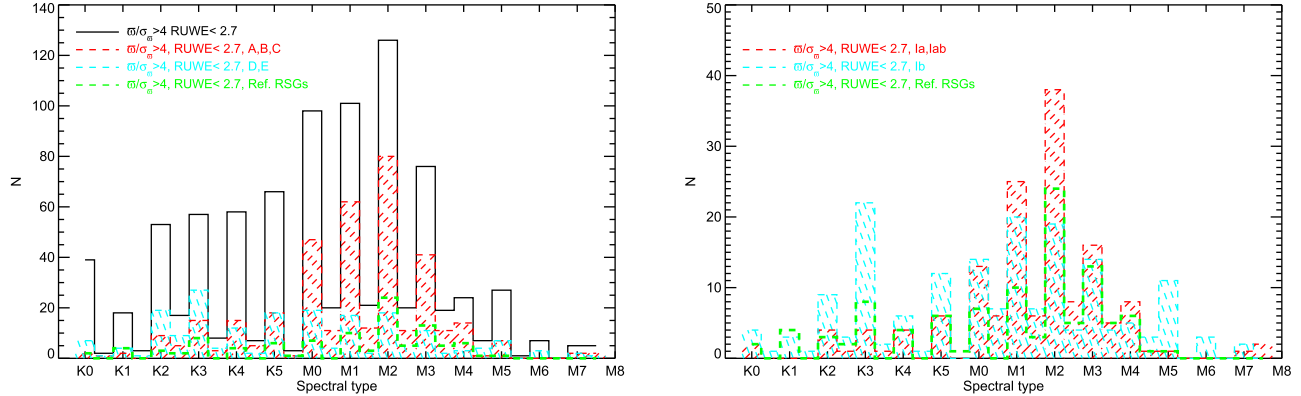
Figure 5. Right panel: in black is the histogram of the spectral types of sources with good distances ($\varpi/\sigma_\varpi(ext) > 4$ and RUWE < 2.7); in red is are sources with $M_{bol} < -5.0$ mag, i.e., located in Area A and B, or in Area C but reported as class I in all previous literature; in cyan is the histogram of sources with $M_{bol} > -5.0$ mag, located in Area D, or in Area E but reported as class I in all previous literature; in green is the histogram of reference RSGs. Right panel: in red are sources of adopted class Ia, Iab and with good distances and $M_{bol} < -3.6$ mag; in cyan is the histogram of sources of adopted class Ib with good distances and $M_{bol} < -3.6$ mag; in green is the histogram of reference RSGs.

(B) Area B contains stars with $-5.0 > M_{bol} > -7.1$ mag and earlier than an M4. This area is rich in stars with masses larger than $7\,M_\odot$.

(C) Area C contains late-type stars with $-5.0 > M_{bol} > -7.1$ mag and later than an M4. This area is expected to be dominated by AGBs (4–9 $M_\odot$).

(D) Area D contains late-type stars with $-3.6 > M_{bol} > -5.0$ mag and bluer than Equation (1). This area contain AGBs of intermediate masses and some faint K-type $9\,M_\odot$ stars at the onset of their cold phase ($M_{bol} = -4.5$ mag).

(E) Area E contains late-type stars with $-3.6 > M_{bol} > -5.0$ mag and redder than Equation (1). This area is expected to be dominated by old and more abundant AGBs (2–3 $M_\odot$).

(F) Area F contains late-type stars with $M_{bol} > -3.6$ mag. Those stars are fainter than the tip of the red giant branch.

In Figure 4, in the theoretical M_{bol} versus T_{eff} diagram, as well as in the observational $K_{so}-DM$ versus J_o-K_{so} diagram, we mark the areas defined above with different colors. These luminosity areas are also added in Table 4. In Figure 5, we show a histogram of the spectral types of the 889 sources with $\varpi/\sigma_\varpi > 4$ and RUWE < 2.7.

Reference RSGs appear to be made by stars with class Ia and Iab (35%), as well as stars with class Ib (33%). In Figures 3 and 5, the distribution of reference RSGs appears similar to that of stars Ia and Iab, with stars falling mostly in Areas A and B; but this differs from class Ib stars, which are sparsely distributed over Areas A, B, C, E, and F.

From Table 1, about 43 sources (5%) are found to be located in Area A ($M_{bol} \lesssim -7.1$ mag). Among them there are two stars, HD 99619 and HD 105563 A, with previously uncertain class. Of the sources, 312 (35%) are located in Area B and are likely more massive than $7\,M_\odot$. About 30% of the sample is made of stars fainter than the tip of the red giant branch (Area F).

A large number of RSGs detected at infrared wavelengths (about 300) were included in the presented compilation; however, for most of those stars parallaxes are not available in DR2 (Table 6 shows only 16 stars from infrared catalogs; e.g., Davies et al. 2008, 2007; Clark et al. 2009; Liermann et al. 2009;

Table 6
Numbers of Collected Stars per Luminosity Class

Sample	N(sp)	N(Ks)	N(plx)	N_A	N_B blue	N_D blue	N_{CE} red	N_F (III)	Nnew(I)
						N(Ks+plx)			
All[a]	1406	1406	889	43	322	134	110	280	35
Ref. opt stars[b]	170	170	135	26	69	21	2	17	0
Ref. IR stars[c]	312	312	16	0	1	3	0	12	1
Nsp(Ia)	57	57	28	12	9	1	4	2	0
Nsp(Iab)	243	243	161	16	90	11	9	35	0
Nsp(Ib)	300	300	259	2	76	52	48	81	0
Nsp(any I)	1013	1013	620	41	253	86	82	158	0
Nsp(I-II)	166	166	113	0	36	24	14	39	0

Notes. N(sp) = number of stars with known available spectral types. N(Ks) = number of stars with available near-infrared measurements. N(plx) = number of stars with ϖ/σ_ϖ(ext) > 4 and RUWE < 2.7. N_A = number of stars located in Area A. N_B = number of stars located in Area B. N_D = number of stars located in Area D. N_{CE} = number of stars located in Areas C or E. N_F = number of stars in Area F. Nnew(I) = number of stars without adopted classes and to which we assign Areas A or B. Nsp(Ia) = number of stars with luminosity classes Ia. Nsp(Iab) = number of stars with luminosity classes Iab. Nsp(Ib) = number of stars with luminosity classes Ib. Nsp(any I) = number of stars with luminosity classes (I, Ia, Iab, Ib). Nsp(I-II) = number of stars with luminosity classes (I-II).
[a] All stars in Table 1.
[b] Example of optically visible RSGs taken from Caron et al. (2003), Levesque et al. (2005), Jura & Kleinmann (1990), Kleinmann & Hall (1986), Elias et al. (1985), and Humphreys (1978).
[c] Example of optically obscured sources taken from Messineo et al. (2017), Clark et al. (2009), Davies et al. (2007, 2008), Negueruela et al. (2010, 2011, 2012), and Liermann et al. (2009).

Table 7
Magnitudes per Spectral Types

Nstar	Sp.Type	M_{bol} (mag)	M_K (mag)	M_V (mag)	M_{bol}-bin (mag)	$V - K$[a]
3	K0.5-K0	-5.71 ± 0.34	-8.12 ± 0.33	-6.86 ± 1.01	$<-5.$	2.16
2	K1.5-K1	-6.04 ± 0.22	-8.50 ± 0.22	-6.77 ± 0.27	$<-5.$	2.29
15	K2.5-K2	-5.74 ± 0.17	-8.25 ± 0.17	-5.97 ± 0.24	$<-5.$	2.44
18	K3.5-K3	-5.60 ± 0.13	-8.15 ± 0.13	-5.37 ± 0.13	$<-5.$	2.72
20	K4.5-K4	-5.75 ± 0.14	-8.35 ± 0.14	-5.00 ± 0.27	$<-5.$	3.00
21	K5.5-K5	-5.60 ± 0.11	-8.24 ± 0.11	-4.63 ± 0.18	$<-5.$	3.70
60	M0.5-M0	-5.72 ± 0.08	-8.42 ± 0.08	-4.31 ± 0.12	$<-5.$	3.79
74	M1.5-M1	-6.02 ± 0.08	-8.76 ± 0.08	-4.44 ± 0.13	$<-5.$	3.92
91	M2.5-M2	-6.29 ± 0.08	-9.09 ± 0.08	-4.50 ± 0.11	$<-5.$	4.11
52	M3.5-M3	-6.62 ± 0.13	-9.47 ± 0.13	-4.03 ± 0.15	$<-5.$	4.58
15	M4.5-M4	-6.40 ± 0.16	-9.29 ± 0.16	-3.58 ± 0.32	$<-5.$	5.24
7	M5.5-M5	-5.47 ± 0.13	-8.43 ± 0.13	-1.90 ± 0.26	$<-5.$	6.06
3	M6.5-M6	-4.43 ± 0.21	-7.52 ± 0.22	0.56 ± 0.93	$[-3.6, -5.0]$	
7	M5.5-M5	-4.14 ± 0.16	-7.10 ± 0.16	0.14 ± 0.35	$[-3.6, -5.0]$	
7	M4.5-M4	-4.12 ± 0.10	-7.01 ± 0.10	-0.95 ± 0.16	$[-3.6, -5.0]$	
13	M3.5-M3	-4.39 ± 0.09	-7.23 ± 0.09	-0.94 ± 0.57	$[-3.6, -5.0]$	
23	M2.5-M2	-4.55 ± 0.07	-7.36 ± 0.07	-2.10 ± 0.25	$[-3.6, -5.0]$	
19	M1.5-M1	-4.28 ± 0.10	-7.01 ± 0.10	-2.39 ± 0.17	$[-3.6, -5.0]$	
21	M0.5-M0	-4.43 ± 0.10	-7.13 ± 0.09	-2.99 ± 0.17	$[-3.6, -5.0]$	
17	K5.5-K5	-4.54 ± 0.10	-7.18 ± 0.10	-2.79 ± 0.25	$[-3.6, -5.0]$	
14	K4.5-K4	-4.57 ± 0.10	-7.17 ± 0.10	-3.93 ± 0.27	$[-3.6, -5.0]$	
31	K3.5-K3	-4.34 ± 0.06	-6.90 ± 0.07	-3.85 ± 0.11	$[-3.6, -5.0]$	
27	K2.5-K2	-4.29 ± 0.07	-6.80 ± 0.07	-4.09 ± 0.10	$[-3.6, -5.0]$	
5	K1.5-K1	-4.16 ± 0.22	-6.63 ± 0.21	-4.37 ± 0.24	$[-3.6, -5.0]$	
8	K0.5-K0	-4.19 ± 0.10	-6.59 ± 0.10	-4.35 ± 0.33	$[-3.6, -5.0]$	

Notes. Average magnitudes of stars in Table 4 with $\varpi/\sigma_\varpi > 4$ and RUWE < 2.7. The errors on the mean values are calculated as $\sqrt{\frac{\sum_{j=0}^{j=N-1}(M_{bol\,j} - \text{mean})^2}{N-1}}) \times \frac{1}{N}$.
At the top are sources with $M_{bol} < -5.0$ mag and Area A or B, or Area C but with secure class I from previous literature. At the bottom are stars with $-3.6 < M_{bol} < -5.0$ mag and Area D, or E (but with secure class I from previous literature).
[a] $V - K$ colors from Johnson (1966). Our $V - K_s$ colors per spectral type are consistent within errors with the $V - K$ colors listed in the review by Johnson (1966), with a mean difference of 0.26 mag and a dispersion around the mean of 0.28 mag.

Table 8
Magnitudes per Spectral Types of Stars with Classes Ia and Iab

Nstar	Sp.Type	M_{bol} (mag)	M_{K} (mag)	M_V (mag)	M_{bol}-bin (mag)
2	K0.5-K0	-5.41 ± 0.97	-7.82 ± 0.96	-6.11 ± 0.27	< -3.6
5	K2.5-K2	-5.65 ± 0.38	-8.18 ± 0.38	-5.86 ± 0.56	< -3.6
5	K3.5-K3	-5.68 ± 0.52	-8.22 ± 0.51	-5.13 ± 0.56	< -3.6
3	K4.5-K4	-5.01 ± 0.11	-7.61 ± 0.11	-3.85 ± 0.14	< -3.6
6	K5.5-K5	-4.99 ± 0.36	-7.65 ± 0.36	-3.66 ± 0.78	< -3.6
19	M0.5-M0	-5.94 ± 0.20	-8.64 ± 0.20	-4.51 ± 0.21	< -3.6
31	M1.5-M1	-5.80 ± 0.11	-8.54 ± 0.11	-4.09 ± 0.22	< -3.6
46	M2.5-M2	-6.35 ± 0.14	-9.15 ± 0.14	-4.58 ± 0.23	< -3.6
21	M3.5-M3	-7.05 ± 0.22	-9.90 ± 0.22	-4.06 ± 0.31	< -3.6
9	M4.5-M4	-6.22 ± 0.39	-9.11 ± 0.38	-3.49 ± 0.53	< -3.6
1	M5.5-M5	-5.33	-8.29	-2.49	< -3.6

Note. Average magnitudes of stars in Table 6 with $\varpi/\sigma_\varpi > 4$ and RUWE < 2.7 and classes Ia and Iab.

Table 9
Magnitudes per Spectral Types of Reference RSGs

Nstar	Sp.Type	M_{bol} (mag)	M_{K} (mag)	M_V (mag)	M_{bol}-bin (mag)
1	K0.5-K0	-4.68	-7.09	-4.77	< -3.6
2	K1.5-K1	-4.43 ± 0.45	-6.89 ± 0.44	-4.67 ± 0.33	< -3.6
7	K2.5-K2	-4.37 ± 0.26	-6.88 ± 0.26	-4.51 ± 0.28	< -3.6
10	K3.5-K3	-5.14 ± 0.33	-7.69 ± 0.33	-4.95 ± 0.26	< -3.6
3	K4.5-K4	-4.92 ± 0.46	-7.51 ± 0.46	-4.80 ± 0.55	< -3.6
7	K5.5-K5	-5.33 ± 0.28	-7.97 ± 0.28	-4.47 ± 0.35	< -3.6
7	M0.5-M0	-5.99 ± 0.16	-8.69 ± 0.16	-4.80 ± 0.20	< -3.6
15	M1.5-M1	-6.31 ± 0.15	-9.05 ± 0.15	-5.00 ± 0.20	< -3.6
32	M2.5-M2	-6.54 ± 0.12	-9.34 ± 0.12	-4.78 ± 0.15	< -3.6
22	M3.5-M3	-7.19 ± 0.20	-10.04 ± 0.20	-4.19 ± 0.24	< -3.6
6	M4.5-M4	-6.57 ± 0.14	-9.46 ± 0.14	-3.43 ± 0.25	< -3.6
1	M5.5-M5	-5.55	-8.51	-2.19	< -3.6

Note. Average magnitudes of stars plotted in the top panels of Figure 3.

Negueruela et al. 2010, 2011, 2012; Messineo et al. 2017).

3.3. Gaia Variables

We searched our sample for the presence of *Gaia* variables and found that only 137 stars of the initial 1342 source with *Gaia* data were flagged as variables (Holl et al. 2018), and 90 out of the 889 have good parallaxes (about 10%). The spectral types of all 90 but 1 have variables ranging from K5 to M7, and 83 of them are automatically classified by the *Gaia* pipeline as long-period variables (LPVs), including Mira and semiregular (SR) stars. Their average variation in the *G*-band is 0.51 mag with a dispersion around the mean of 0.38 mag, including two stars with variations above 2.5 mag (0.1%), which are in Areas C and E. There are 65 (out of 90) variables in Areas A and B; their variations in the *G*-band range from 0.2 to 0.8 mag, with a mean variation of 0.41 mag and dispersion around the mean of 0.14 mag. Similar values are found with the 9 variables of class Ib (a mean of 0.46 mag and a $\sigma = 0.33$ mag). There are 9 variables fainter than $M_{\mathrm{bol}} > -3.6$ mag (Area F), with 7 of them later than M5. Their mean variation is 0.63 mag and $\sigma = 0.45$ mag.
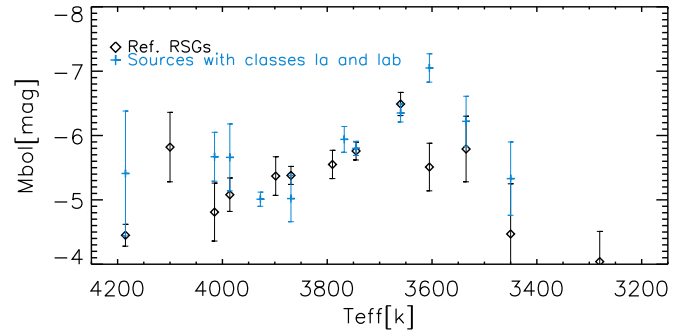

Figure 6. Average M_{bol} vs. T_{eff}. The cyan crosses show the values for class Ia and Iab stars. The black diamonds indicate the values for the reference RSGs.

An analysis of the *G*-band light curves will be presented elsewhere.

3.4. Average Magnitudes per Spectral Type

In Table 7 we present average magnitudes per spectral type of stars of class I and with $M_{\mathrm{bol}} < -5.0$ mag, and of stars with $-3.6 < M_{\mathrm{bol}} < -5.0$ mag. This table is useful for Galactic star counts (e.g., Wainscoat et al. 1992). In Table 2 of Just et al. (2015), infrared luminosities of *Hipparcos* stars per classes are also provided; for example, their K-M2 I-II stars have
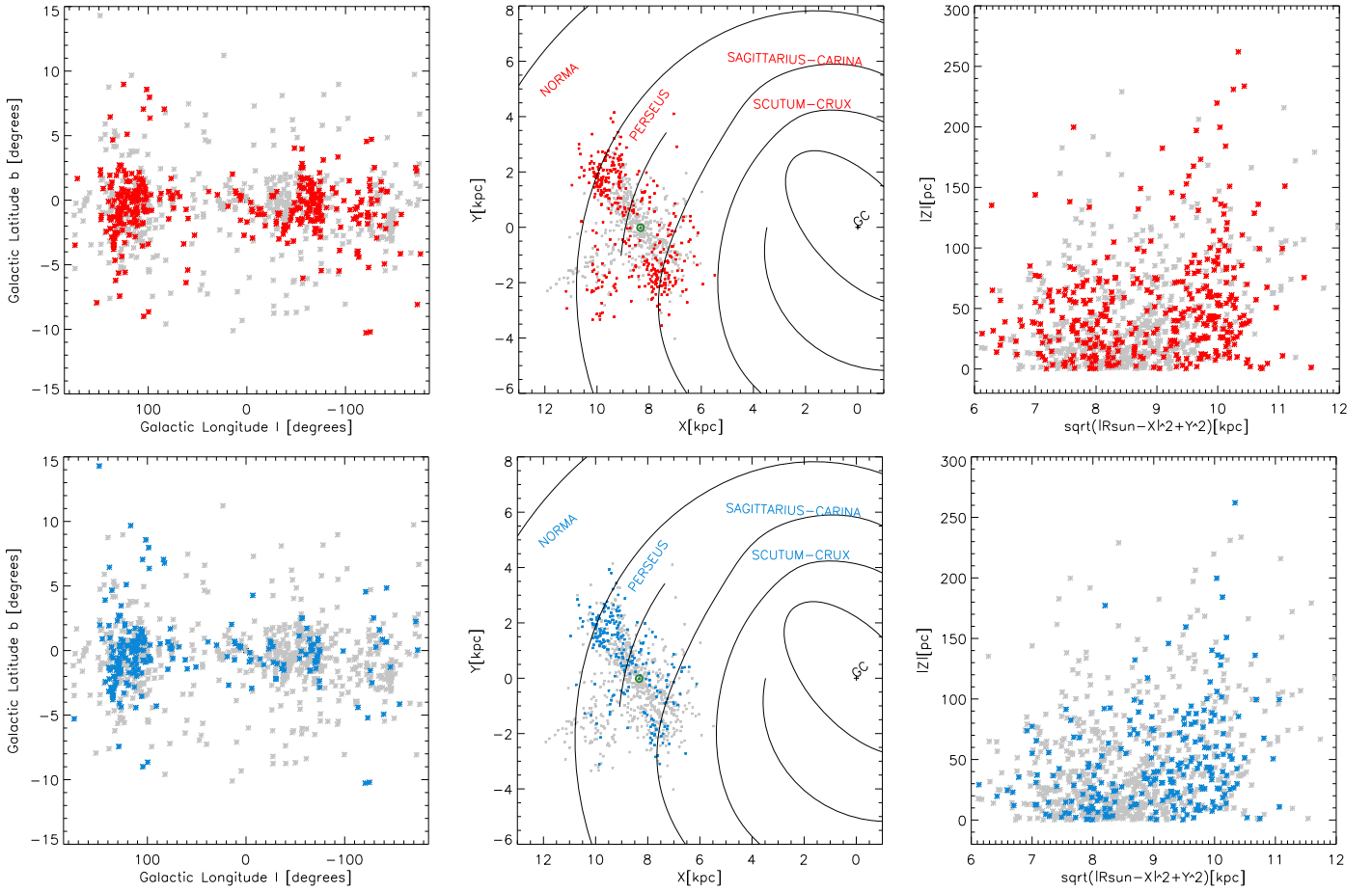
Figure 7. Top left panel: latitudes vs. longitudes of the bright late-type stars in Table 1. Candidate RSGs with $M_{bol} < -5.0$ mag (Area A and B) and ϖ/σ_ϖ(ext) > 4 and RUWE < 2.7 are marked in red. Top middle panel: Galactocentric coordinates XY on the disk of the Milky Way. The Sun location (8.5, 0) is marked in green, while the Galactic Center (GC), marked with a black cross, is at (0, 0). The spiral arms are taken from the work of Cordes & Lazio (2003). Top right panel: distances from the plane $|Z|$ vs. galactocentric distances. Bottom panels: same as the top panels, but this time the cyan asterisks mark bright late-type stars in Table 1 with class Ia or Iab, or reference RSGs (see Figure 3).

$M_K = -9$ mag. For stars with spectral types K-M2 I and $M_{bol} < -5.0$ mag, Table 7 provides an average $M_K = -8.40$ mag with $\sigma = 0.39$ mag.

Additionally, in Tables 8 and 9 we present average magnitudes per spectral type of stars of classes Ia and Iab and of stars in the reference RSG sample.

In Figure 6, we plot the calculated average magnitudes per spectral types of stars with classes Ia and Iab, as well as of stars in the reference RSG sample, versus the T_{eff} values. T_{eff} were estimated from the spectral types with the temperature scale given by Levesque et al. (2005). For stars with T_{eff} from 3650 k to 3950 k, M_{bol} values seem to decrease with decreasing T_{eff} values.

3.5. Spatial Distribution

The bright cool stars analyzed here span 360° of longitude (Figure 7). By using the estimates of distances in Table 1, we obtained the distribution on the Galactic plane shown in Figure 7. Late-type stars brighter than $M_{bol} = -5.0$ mag ($0.8 \times 10^4 L_\odot$) appear radially more distant from the Sun than the whole sample, with heliocentric distances ranging from ≈ 200 to ≈ 4600 pc. Star eta Per (K3 Ib-II) is 239 pc away from us ($\varpi = 4.21 \pm 0.37$ mas), and HD 200905 (K4.5 I) is 283 pc away ($\varpi = 3.59 \pm 0.42$ mas). Antares (alpha Sco, M1.5 Iab),

with an estimated distance of ≈ 170 pc, does not yet have a *Gaia* parallax measurement. PER286 (M2.0 Ib) has an estimated distance of 4.2 kpc ($\varpi = 0.20 \pm 0.04$ mas).

4. Summary

In order to create a catalog of stars with luminosity class I, candidate RSGs, from *Gaia* DR2, we collected 1406 bright late-type stars with at least one spectroscopic record as class I. Spectral types were taken from the collection by Skiff (2014), and in the majority of cases appeared within the uncertainty of 2 subclasses (i.e., the range of types reported for a single entry). For well-known sources, such as those analyzed by Dorda et al. (2016, 2018), Levesque et al. (2005), Jura & Kleinmann (1990), Elias et al. (1985), and Humphreys (1978), spectral types and luminosity classes were taken from these works. At the present time, only a fraction equal to 13% of this sample is known to be associated with open clusters. For each source, we collected available photometric measurements from 2MASS, CIO, *MSX*, *WISE*, MIPSGAL, GLIMPSE, and NOMAD catalogs and estimated their apparent bolometric magnitudes.

We retrieved parallaxes for 1342 sources from *Gaia* DR2, of which 1290 have a $(G_{BP} - G_{RP})$ color. After a data filtering based on signal to noise and astrometric quality ($\varpi/\sigma_\varpi > 4$

and RUWE < 2.7), we were left with a best-quality sample of 889 sources.

With the parallactic distances, we were able to estimate the stellar luminosities, and to build M_{bol} versus T_{eff} diagrams of stars with different classes.

The Galactic catalog of RSGs, i.e., of very likely massive stars because of luminosity and associations with OB stars, by Humphreys (1978), Elias et al. (1985), Jura & Kleinmann (1990), Levesque et al. (2005), Caron et al. (2003) contains 170 stars. Of these reference RSGs, 118 had good parallaxes in DR2 and $M_{bol} < -3.6$ mag. While these reference RSGs appear to contain stars of class Ia, Iab (40%) as well as class Ib (31%), their distribution on the M_{bol} versus T_{eff} diagrams resembles that of class Ia, Iab, with 81% of them located in Areas A and B. Only 44% of class Ib stars with $M_{bol} < -3.6$ mag fall in Areas A and B.

For 609 stars (68% of 889 analyzed stars), M_{bol} values were found to be smaller (brighter) than -3.6 mag, with 536 of them already having been reported in previous literature exclusively as classes I or II. Of these, 5% appear to be highly probable massive stars (stars in Area A), while 41% of them are stars in Area As and B, and are likely more massive than $7\,M_{\odot}$.

A fraction equal to $\approx$30% of the sample appears to be made of stars fainter than the tip of the giant branch (Area F).

A natural output of this luminosity exercise is a tabulated average of absolute magnitudes of luminous late-type stars and RSGs per spectral type. This finer grid of magnitudes will help to predict distances of extragalactic luminous late-type stars.

This catalog is a small demonstration of the cumulative spectroscopic knowledge available in support of the *Gaia* mission. The catalog is useful for high-resolution follow-up spectroscopy, such as, for example, that seen in ongoing large spectroscopic surveys such as LAMOST and GALAH. This is important to understand the evolution and nucleosynthesis occurring in RSGs and massive AGBs (and super-AGB stars). Luminosities, spectral types, and chemistry are key ingredients for an improved study of the Galactic structure and its recent history.

Appendix
Notes on Photometric Data

Typically, initial coordinates by Skiff (2014) are good to within a few arcseconds. A few coordinates were corrected with SIMBAD. An iterative process was needed to make sure we properly identified the counterparts at different wavelengths. The Galactic plane is crowded with sources.

For stars at longitude $|l| > 1°$ and latitude $|l| > 0°.5$, measurements were automatically associated with a selection of good flags to ensure quality. *MSX* upper limits measurements were discarded, and *WISE* sources were chosen with a minimum signal to noise larger than 2. GLIMPSE matches were associated with a magnitude cut at 10 mag, and when a *WISE* source existed, positional coincidence was inspected. The searched stars were usually the brightest at near- and mid-infrared wavelengths, and chart identification was easy. 2MASS matches follow those in the *WISE* and GLIMPSE catalogs. Due to saturation and centroid problems, a few 2MASS identifications had to be fixed (e.g., BD+54 315, VY CMa, Cl* Westerlund 1 26, MZM29, MZM33, RSGC1-F08, IRAS 17433−1750). For stars HD 126152, HD 149812, HD 227793, and BD +36 4025, which have quality parallaxes but no 2MASS errors, we assumed an error in $K_s = 0.8$ mag (see the quality flag provided in Table 4). For omi02 Cyg, *JK* photometry was taken from Morel & Magnenat (1978). For stars [MMF2014] 78, [MFD2010] 5, [GLIMPSE9]-6, and [MMF2014] 46/[MFD2010] 8, *HST HK* data were available (Messineo et al. 2010); for the faint OGLE BW3 V 93508, near-infrared magnitudes are from Lucas et al. (2008). For the highly crowded central region ($|l| < 1°.0$ and $|b| < 0°.5$), only the K-band photometry of Liermann et al. (2009) is provided, and for stars IRC−30320, IRC−30322, [RHI84] 10−565, MZM115 the 2MASS photometry. For LHO036, which has a parallax, additional *JH* measurements were taken from the work of Stolte et al. (2015).

Matches were confirmed with a visual inspection of 2MASS and *WISE* images, as well as of their SEDs. After the visual inspection, a few measurements were discarded because of poor quality (e.g., confused, highly saturated, or strong background emission) and were not compatible with the SED. For stars [MMF2014] 46, GLIMPSE9-6, RSGC2-8, RSGC2-14, 2MASS J18451760-0343051, and 2MASS J18451722-0343136, *MSX* matches were removed. For stars Cl* Westerlund 1 20, Cl* Westerlund 1 75, [MMF2014] 46, GLIMPSE9-6, RSGC1-F08, RSGC1-F05, and RSGC1-F01, *WISE* matches were removed because they are blended with other sources. For stars [HSD93b] 48, [MNG2014] vdB-H 222 778, [MNG2014] vdB-H 222 664, [MNG2014] vdB-H 222 479, [MMF2014] 78, 2MASS J18410261−0552582, HD 195214, and 2MASS J18392955−0544222 only *W*4 measurements were removed because sources were too faint or confused at this longer wavelength. For stars 2MASS J17361839-2217306, RSGC1-F07,

RSGC1-F10, RSGC1-F03, and 2MASS J18395282-0535172, both $W3$ and $W4$ magnitudes were discarded. For HD 14580 and Cl* Westerlund 1 26, $W1$ and $W2$ magnitudes did not fit their SED.

ORCID iDs

M. Messineo ● https://orcid.org/0000-0002-7198-1518
A. G. A. Brown ● https://orcid.org/0000-0002-7419-9679

References

Alard, C., Blommaert, J. A. D. L., Cesarsky, C., et al. 2001, ApJ, 552, 289
Alonso-Santiago, J., Negueruela, I., Marco, A., et al. 2017, MNRAS, 469, 1330
Asaki, Y., Deguchi, S., Imai, H., et al. 2010, ApJ, 721, 267
Bailer-Jones, C. A. L. 2015, PASP, 127, 994
Bailer-Jones, C. A. L., Rybizki, J., Fouesneau, M., Mantelet, G., & Andrae, R. 2018, AJ, 156, 58
Benjamin, R. A., Churchwell, E., Babler, B. L., et al. 2005, ApJL, 630, L149
Blanco, V. M., McCarthy, M. F., & Blanco, B. M. 1984, AJ, 89, 636
Blum, R. D., Ramírez, S. V., Sellgren, K., & Olsen, K. 2003, ApJ, 597, 323
Brogaard, K., VandenBerg, D. A., Bedin, L. R., et al. 2017, MNRAS, 468, 645
Cambrésy, L., Genova, F., Wenger, M., et al. 2011, EAS Publications Ser., 49, 135
Caron, G., Moffat, A. F. J., St-Louis, N., Wade, G. A., & Lester, J. B. 2003, AJ, 126, 1415
Chen, X., Shen, Z.-Q., & Xu, Y. 2007, ChJAA, 7, 531
Chiavassa, A., Pasquato, E., Jorissen, A., et al. 2011, A&A, 528, A120
Chieffi, A., & Limongi, M. 2013, ApJ, 764, 21
Choi, Y. K., Hirota, T., Honma, M., et al. 2008, PASJ, 60, 1007
Churchwell, E., Babler, B. L., Meade, M. R., et al. 2009, PASP, 121, 213
Clark, J. S., Negueruela, I., Davies, B., et al. 2009, A&A, 498, 109
Comerón, F., Torra, J., Chiappini, C., et al. 2004, A&A, 425, 489
Cordes, J. M., & Lazio, T. J. W. 2003, arXiv:astro-ph/0301598
Cordier, D., Pietrinferni, A., Cassisi, S., & Salaris, M. 2007, AJ, 133, 468
Cutri, R. M., Skrutskie, M. F., van Dyk, S., et al. 2003, 2MASS All Sky Point Sources Catalog (Washington, DC: NASA), http://irsa.ipac.caltech.edu/applications/Gator/
Davidson, K., Helmel, G., & Humphreys, R. M. 2018, RNAAS, 2, 133
Davies, B., Figer, D. F., Kudritzki, R.-P., et al. 2007, ApJ, 671, 781
Davies, B., Figer, D. F., Law, C. J., et al. 2008, ApJ, 676, 1016
Davies, B., Origlia, L., Kudritzki, R.-P., et al. 2009, ApJ, 696, 2014
Doherty, C. L., Gil-Pons, P., Siess, L., Lattanzio, J. C., & Lau, H. H. B. 2015, MNRAS, 446, 2599
Dorda, R., González-Fernández, C., & Negueruela, I. 2016, A&A, 595, A105
Dorda, R., Negueruela, I., & González-Fernández, C. 2018, MNRAS, 475, 2003
Egan, M. P., Price, S. D., Kraemer, K. E., et al. 2003, yCat, 5114
Eggenberger, P., Meynet, G., & Maeder, A. 2002, A&A, 386, 576
Ekström, S., Georgy, C., Eggenberger, P., et al. 2012, A&A, 537, A146
Elias, J. H., Frogel, J. A., & Humphreys, R. M. 1985, ApJS, 57, 91
ESA (ed.) 1997, in ESA Special Publication, 1200
Ferraro, F. R., Montegriffo, P., Origlia, L., & Fusi Pecci, F. 2000, AJ, 119, 1282
Figer, D. F., MacKenty, J. W., Robberto, M., et al. 2006, ApJ, 643, 1166
Gaia Collaboration, Brown, A. G. A., Vallenari, A., et al. 2018, A&A, 616, A1
Gaia Collaboration, Prusti, T., de Bruijne, J. H. J., et al. 2016, A&A, 595, A1
Gehrz, R. 1989, in IAU Symp. 135, Interstellar Dust, ed. L. J. Allamandola & A. G. G. M. Tielens (Dordrecht: Kluwer), 445

Gezari, D. Y., Pitts, P. S., Schmitz, M., & Mead, J. M. 1996, yCat, 2209
Glass, I. S., & Feast, M. W. 1973, MNRAS, 163, 245
Gray, R. O., & Corbally, J. 2009, Stellar Spectral Classification (Princeton, NJ: Princeton Univ. Press)
Gutermuth, R. A., & Heyer, M. 2015, AJ, 149, 64
Holl, B., Audard, M., Nienartowicz, K., et al. 2018, A&A, 618, A30
Humphreys, R. M. 1978, ApJS, 38, 309
Iben, I., Jr. 1974, ARA&A, 12, 215
Johnson, H. L. 1966, ARA&A, 4, 193
Josselin, E., & Plez, B. 2007, A&A, 469, 671
Jura, M., & Kleinmann, S. G. 1990, ApJS, 73, 769
Just, A., Fuchs, B., Jahreiß, H., et al. 2015, MNRAS, 451, 149
Kleinmann, S. G., & Hall, D. N. B. 1986, ApJS, 62, 501
Koornneef, J. 1983, A&A, 128, 84
Kusuno, K., Asaki, Y., Imai, H., & Oyama, T. 2013, ApJ, 774, 107
Levesque, E. M., Massey, P., Olsen, K. A. G., et al. 2005, ApJ, 628, 973
Liermann, A., Hamann, W.-R., & Oskinova, L. M. 2009, A&A, 494, 1137
Lindegren, L., Hernández, J., Bombrun, A., et al. 2018, A&A, 616, A2
Lucas, P. W., Hoare, M. G., Longmore, A., et al. 2008, MNRAS, 391, 136
Luri, X., Brown, A. G. A., Sarro, L. M., et al. 2018, A&A, 616, A9
Massey, P., DeGioia-Eastwood, K., & Waterhouse, E. 2001, AJ, 121, 1050
Mengel, S., & Tacconi-Garman, L. E. 2007, A&A, 466, 151
Mermilliod, J. C., Mayor, M., & Udry, S. 2008, A&A, 485, 303
Messineo, M., Figer, D. F., Davies, B., et al. 2008, ApJL, 683, L155
Messineo, M., Figer, D. F., Davies, B., et al. 2010, ApJ, 708, 1241
Messineo, M., Habing, H. J., Menten, K. M., et al. 2005, A&A, 435, 575
Messineo, M., Zhu, Q., Ivanov, V. D., et al. 2014, A&A, 571, A43
Messineo, M., Zhu, Q., Menten, K. M., et al. 2016, ApJL, 822, L5
Messineo, M., Zhu, Q., Menten, K. M., et al. 2017, ApJ, 836, 65
Montegriffo, P., Ferraro, F. R., Origlia, L., & Fusi Pecci, F. 1998, MNRAS, 297, 872
Moravveji, E., Guinan, E. F., Khosroshahi, H., & Wasatonic, R. 2013, AJ, 146, 148
Morel, M., & Magnenat, P. 1978, A&AS, 34, 477
Morgan, W. W., Keenan, P. C., & Kellman, E. 1943, An Atlas of Stellar Spectra, with an Outline of Spectral Classification (Chicage, IL: Univ. Chicago Press)
Negueruela, I., González-Fernández, C., Marco, A., & Clark, J. S. 2011, A&A, 528, A59
Negueruela, I., González-Fernández, C., Marco, A., Clark, J. S., & Martínez-Núñez, S. 2010, A&A, 513, A74
Negueruela, I., Marco, A., González-Fernández, C., et al. 2012, A&A, 547, A15
Pasquato, E., Pourbaix, D., & Jorissen, A. 2011, A&A, 532, A13
Price, S. D., Egan, M. P., Carey, S. J., Mizuno, D. R., & Kuchar, T. A. 2001, AJ, 121, 2819
Rayner, J. T., Cushing, M. C., & Vacca, W. D. 2009, ApJS, 185, 289
Skiff, B. A. 2014, yCat, 2023
Skrutskie, M. F., Cutri, R. M., Stiening, R., et al. 2006, AJ, 131, 1163
Stolte, A., Hußmann, B., Olczak, C., et al. 2015, A&A, 578, A4
Sweigart, A. V., Greggio, L., & Renzini, A. 1990, ApJ, 364, 527
Vassiliadis, E., & Wood, P. R. 1993, ApJ, 413, 641
Verheyen, L., Messineo, M., & Menten, K. M. 2012, A&A, 541, A36
Verhoelst, T., van der Zypen, N., Hony, S., et al. 2009, A&A, 498, 127
Wainscoat, R. J., Cohen, M., Volk, K., Walker, H. J., & Schwartz, D. E. 1992, ApJS, 83, 111
Wright, E. L., Eisenhardt, P. R. M., Mainzer, A. K., et al. 2010, AJ, 140, 1868
Xu, S., Zhang, B., Reid, M. J., et al. 2018, ApJ, 859, 14
Zacharias, N., Monet, D. G., Levine, S. E., et al. 2005, yCat, 1297
Zhang, B., Reid, M. J., Menten, K. M., & Zheng, X. W. 2012, ApJ, 744, 23